

Shape-free theory for the self-assembly kinetics in macromolecular systems

L. F. Trugilho and L. G. Rizzi

*Departamento de Física, Universidade Federal de Viçosa (UFV),
Av. P. H. Rolfs, s/n, 36570-900, Viçosa, Brazil.*

Self-assembly kinetics is usually described by approaches which assume that the shape of the aggregates has a definite form (*e.g.*, spherical, cylindrical, cubic, etc), however that is unlikely to be the case in many finite-sized macromolecular and colloidal systems. Here we consider a simple aggregation model which displays a first-order phase transition in order to illustrate a rate theory based on microcanonical analysis that allows one to obtain a shape-free description of its self-assembly kinetics. Stochastic simulations are performed to validate our approach and demonstrate how the equilibrium thermostistical properties of the system can be related to the temperature-dependent rate constants. As a model-independent kinetic approach, it may provide experimentalists a reliable method to reconstruct free-energy profiles and microcanonical entropies from kinetic data.

Self-assembly kinetics is of particular interest to a myriad of scientific areas, ranging from climate and materials sciences to soft matter physics and biology [1]. Nucleation, in particular, occurs when the system present interactions that lead to first-order phase transitions, and these can be associated not only to, *e.g.*, size-dependent recalescence phenomena in phase change materials [2], but also to many human diseases that are related to misfolded protein aggregation [3]. Although several attempts to adapt the classical nucleation theory to finite molecular systems have been made (*e.g.*, [4, 5]), most of them are based either on the capillarity approximation or on the precary assumption that the shape of the aggregates has spherical symmetry. However, it may be difficult to imagine that spherically symmetric aggregates are the case when considering, for instance, some biopolymeric systems [6]. In fact, even for the simplest Ising-like models one may get into trouble when applying the classical theory to systems where molecules present, *e.g.*, anisotropic interactions [7, 8].

Recently, the authors of Ref. [9] explored the alternative idea that free-energy barriers extracted from the microcanonical entropy $S(N, V, E)$ could be used in an Arrhenius-like expression, *i.e.*, proportional to $e^{-\Delta G^\ddagger/k_B T}$, to provide a shape-free theory for the self-assembly rates in different molecular systems (*i.e.*, Lennard-Jones colloids and polymeric chains). It could have been a promising approach since equilibrium properties like ΔG^\ddagger have been already determined by this type of microcanonical shape-free approach in many other finite-sized molecular systems which present first-order phase transitions through advanced computational simulations techniques (*e.g.*, multicanonical [10, 11], entropic sampling [12], Wang-Landau [13], and statistical temperature [14–16]). To name a few examples we could mention polymer adsorption [17, 18] and condensation [19], protein folding [20–23] and dimerization [24, 25], droplet condensation-evaporation [26], and peptide aggregation [27–30]. Unfortunately, the approach considered in Ref. [9], just like the one in Ref. [22], is restricted to the self-assembly kinetics at a temperature equal to the transition temperature T^* . The full

temperature-dependent expressions for the rate constants was only obtained recently in Ref. [31], where the proposed rate theory was able to successfully describe results from both protein folding and ice nucleation experiments.

Here we discuss how one can use microcanonical thermostatics analysis [19, 32] as a shape-free and model-independent method to determine the self-assembly rate constants of macromolecular and colloidal systems that display first-order phase transitions. We illustrate our discussion by considering a simple aggregation model for which the density of states $\Omega(E)$, hence $S(N, V, E) = k_B \ln \Omega(E)$, can be obtained analytically.

As it is schematically shown in Fig. 1(a), the model consists of N molecules that are inside a fixed volume V , which is divided into two arbitrary volumes, V_0 and $V' = V - V_0$. We assume that the n molecules that are inside the volume V_0 contribute with an interaction energy given by $E_p(n) = -\nu g(n)$, where $g(n) = (n^\alpha - 1)$ is the number of bonds with effective strength ν between the n molecules. The total energy of all molecules in the system is given by $E = E_k + E_p$, with E_k being the sum of their kinetic energies. We consider that the molecules in the remaining volume V' are diluted enough so that they do not interact with each other. Hence, at a given energy E , the density of states can be evaluated as

$$\Omega(E) \propto \sum_{n=n_{\min}}^N \frac{e^{\eta(N-n)}}{n!(N-n)!} (E + \nu g(n))^{3N/2} \quad , \quad (1)$$

where $\eta = \ln((V - V_0)/V_0)$ and n_{\min} is the minimum number of molecules that is required to be inside V_0 if E is negative (note that E_k is always positive and, if $E > 0$, then $n_{\min} = 1$). Because the general ideas that lead to Eq. 1 are similar to those used in Ref. [33], a detailed presentation of it (including the phase diagram of the model) will be discussed elsewhere [34]. But, it is worth mentioning that the case $\alpha = 2$ corresponds to a mean-field long-range interacting model known as the Thirring's model [35, 36], while the case $\alpha = 1$ represent a linear-like polymeric system where the molecules interact only with their nearest-neighbors.

By considering the Stirling's approximation [37], and

taking the number $\bar{n} = \bar{n}(E)$ that maximizes the sum in Eq. 1 (see Fig. 1(a)), the microcanonical entropy can be computed as $S(E) \equiv S(E, \bar{n}) = k_B \ln \Omega(E, \bar{n})$. Hence, the microcanonical temperature can be evaluated as $T(E) = 1/k_B b(E)$, where

$$b(E) = \frac{1}{k_B} \left(\frac{\partial S(E)}{\partial E} \right)_{N,V}, \quad (2)$$

with k_B being the Boltzmann constant. Figures 1(a) and 1(b) show, respectively, $\bar{n}(E)$ and $T(E)$ for a system with $N = 10^4$ molecules, $\alpha = 1.2$, $\nu = 3.011$ kJ/mol (*i.e.*, 5×10^{-21} J per effective bond), and $\eta = 7.7$. The resulting S-shaped caloric curve obtained for $T(E)$ displayed in Fig. 1(b) indicates that the phase transition takes place at a temperature $T^* = 314.626$ K (*i.e.*, $\sim 41.5^\circ\text{C}$). The transition temperature separates a high-temperature phase where most of the molecules are dissolved in volume V' , and a low-temperature phase, where the system is found at energies closer to E_- , with an aggregate containing \bar{n} molecules formed inside the volume V_0 (see the schematic drawing in Fig. 1(a)). It is important to emphasize that the model does not require any arbitrary information about the shape of the volume V_0 . Even so, the value $\alpha < 2$ is used here as an effective way to indicate that some of the molecules must be attached to the periphery of the aggregate. In order to obtain experimentally relevant physical units, we consider that each molecule have a fixed volume v_m , so that the interacting volume is given by $V_0 = N v_m \approx 4.19 \times 10^4 \text{ nm}^3$, and the molar concentration of solute is estimated as $c = N/(N_A V) = \rho/N_A v_m = 179 \mu\text{M}$, with N_A being the Avogadro's constant and $\rho = V_0/V = (1 + e^\eta)^{-1} \approx 4.526 \times 10^{-4}$, *i.e.*, $V \approx 9.25 \times 10^7 \text{ nm}^3$.

At the inverse transition temperature $\beta^* = 1/N_A k_B T^*$ of first-order phase transitions, the canonical probability density function (PDF), $p(E) \propto e^{-\beta^* F(E)}$, present two maxima at energies E_- and E_+ , and one minimum at E^* , which correspond to the two minima and one maximum in the energy-dependent free-energy $\beta^* F(E) = \beta^* E - S(E)/k_B$, respectively. Thus, the free-energy profile that is shown in Fig. 1(c) can be obtained by considering

$$\beta^* \Delta F(E) = \beta^* F(E) - \beta^* F(E_-) = (S^*(E) - S(E))/k_B, \quad (3)$$

where $S^*(E) = k_B \beta^* (E - E_-) + S(E_-)$, so that $\beta^* = k_B^{-1} (S(E_+) - S(E_-))/\Delta E^\dagger$, with $S^*(E_+) \equiv S(E_+)$, and $\Delta E^\dagger = E_+ - E_-$ being the microcanonical latent heat.

Now, in order to obtain analytical expressions for the forward κ_- and reverse κ_+ rate constants, we follow the approach discussed in Refs. [38, 39], and compute the mean-first passage times (MFPT) τ_- and τ_+ directly from estimates for the canonical PDF $p(E)$. For instance, the MFPT τ_- which takes for the system to go from the energy E_+ to E_- can be evaluated as

$$\tau_- = \frac{1}{D} \int_{E_-}^{E_+} \frac{dE}{p(E)} \int_E^\infty p(E') dE' \approx \frac{4\pi\tau_\varepsilon}{\varepsilon^2 \sqrt{\gamma^* \gamma_+}} \frac{\Gamma_+(\beta)}{\Gamma^*(\beta)}, \quad (4)$$

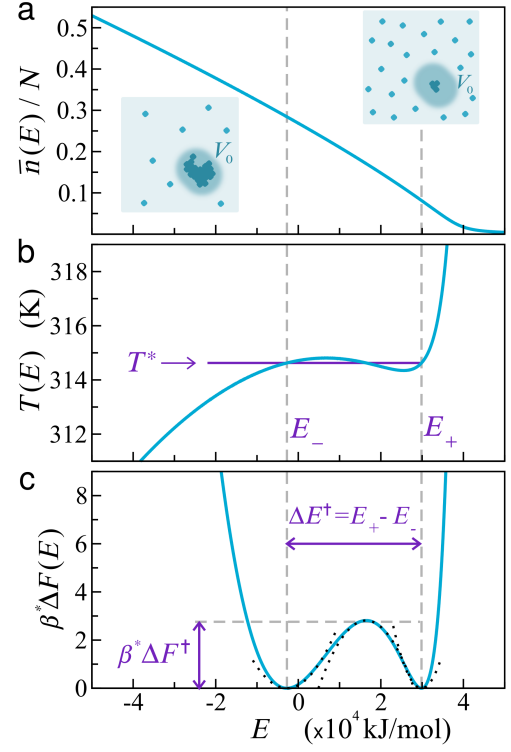


FIG. 1. (a) Ratio between the number of particles in the aggregate $\bar{n}(E)$ and the total number of particles N , (b) microcanonical temperature $T(E)$, and (c) free-energy profile at the transition $\beta^* \Delta F(E)$, Eq. 3. Results were obtained for $N = 10^4$, $\alpha = 1.2$, $\nu = 3.011$ kJ/mol, and $\eta = 7.7$. In (b) the horizontal purple line indicate the transition temperature $T^* = 314.626$ K determined through a Maxwell-like construction, while the purple arrows in (c) denote the free-energy barrier, $\beta^* \Delta F^\dagger = 2.813$, and the microcanonical latent heat, $\Delta E^\dagger = E_+ - E_- = 3.258 \times 10^4$ kJ/mol. Dotted lines in (c) are quadratic approximated expressions for $\beta^* \Delta F(E)$ (see text).

where $D = \varepsilon^2/2\tau_\varepsilon$ is a diffusion coefficient in the energy space that is defined in terms of ε and τ_ε , which are the typical energy and time scales involved in the microscopic energy exchange between the N molecules and the thermal reservoir (*i.e.*, implicitly solvent); similarly, the MFPT for the system to go from the energy E_- to E_+ is $\tau_+ \approx 4\pi\tau_\varepsilon\Gamma_-(\beta)/(\varepsilon^2\sqrt{\gamma^*\gamma_-}\Gamma^*(\beta))$, where the factors $\Gamma^*(\beta)$ and $\Gamma_\pm(\beta)$ are given, respectively, by

$$\Gamma^*(\beta) = \exp \left[-\beta^* \Delta F^\dagger + \frac{S^*(E_-)}{k_B} - \beta^* E_- - \frac{[(\beta - \beta^*) + \gamma^* E^*]^2}{2\gamma^*} + \frac{\gamma^*(E^*)^2}{2} \right], \quad (5)$$

and

$$\Gamma_\pm(\beta) = \exp \left[\frac{S^*(E_-)}{k_B} - \beta^* E_- + \frac{[(\beta - \beta^*) - \gamma_\pm E_\pm]^2}{2\gamma_\pm} - \frac{\gamma_\pm(E_\pm)^2}{2} \right]. \quad (6)$$

These factors in $p(E)$ can be obtained by writing the microcanonical entropy as $S(E) = S^*(E) - k_B \beta^* \Delta F(E)$,

and expanding the free-energy profile $\beta^* \Delta F(E)$ around the energies E_{\pm} as $\beta^* \Delta F(E) \approx (\gamma_{\pm}/2)(E - E_{\pm})^2$, and around E^* as $\beta^* \Delta F(E) \approx \beta^* \Delta F^{\ddagger} - (\gamma^*/2)(E - E^*)^2$, with $\beta^* \Delta F^{\ddagger}$ being a free-energy barrier, as indicated in Fig. 1(c). A numerical fit of these approximated quadratic expressions to the data displayed in Fig. 1(c) (see dotted lines) yields, *e.g.*, $\gamma^* \approx 4.2 \times 10^{-8} (\text{mol/kJ})^{-2}$ for $\beta^* \Delta F(E)$ close to its maximum at E^* .

By considering the above MFPT one can compute the forward and reverse rate constants, respectively, as

$$\kappa_{-} = \frac{1}{\tau_{-}} \approx A_{+} \exp \left[-\Delta E_{+}^{\ddagger} (\beta - \beta^*) - \frac{\bar{\gamma}_{+}}{2} (\beta - \beta^*)^2 \right], \quad (7)$$

and

$$\kappa_{+} = \frac{1}{\tau_{+}} \approx A_{-} \exp \left[-\Delta E_{-}^{\ddagger} (\beta - \beta^*) - \frac{\bar{\gamma}_{-}}{2} (\beta - \beta^*)^2 \right], \quad (8)$$

where $\Delta E_{\pm}^{\ddagger} = E^* - E_{\pm}$ and $\bar{\gamma}_{\pm} = (\gamma_{\pm})^{-1} + (\gamma^*)^{-1}$, with the pre-factors given by $A_{\pm} = (\varepsilon^2/4\pi\tau_{\varepsilon})\sqrt{\gamma^*\gamma_{\pm}}e^{-\beta^*\Delta F^{\ddagger}}$. Here it is worth noting that, for the particular case where $\beta = \beta^*$, the above rate constants are indeed proportional to $e^{-\beta^*\Delta F^{\ddagger}}$, as empirically suggested in Refs. [9, 22]. In addition, one can use the above expressions to evaluate the equilibrium rate constant as

$$\kappa_{\text{eq}} = \frac{\kappa_{-}}{\kappa_{+}} \approx A \exp \left[\Delta E^{\ddagger} (\beta - \beta^*) + \frac{\Delta\bar{\gamma}}{2} (\beta - \beta^*)^2 \right], \quad (9)$$

where $A = \sqrt{\gamma_{+}/\gamma_{-}}$, $\Delta E^{\ddagger} = E_{+} - E_{-}$, and $\Delta\bar{\gamma} = \bar{\gamma}_{-} - \bar{\gamma}_{+} = (\gamma_{-})^{-1} - (\gamma_{+})^{-1}$.

In order to validate our theoretical approach we have implemented stochastic simulations similar to those described in Ref. [31], which yield energy time series that lead to stationary distributions given by the canonical PDF, $p(E_j) = \Omega(E_j)e^{-\beta E_j}/\mathcal{Z}(\beta)$, at discretized energy values, *i.e.*, $E_j = E_0 + j\varepsilon$ with $E_0 = -\nu(N^{\alpha} - 1)$ and $\varepsilon = 30.11 \text{ kJ/mol}$, and $\mathcal{Z}(\beta) = \sum_j \Omega(E_j)e^{-\beta E_j}$ being the canonical partition function [40]. In contact with a thermal reservoir at a temperature close to the transition temperature, the energy fluctuates and the system is able to visit both phases [31]. Hence, one can evaluate the MFPTs τ_{-} and τ_{+} numerically by considering the labelled walkers (or coloring/milestoning [39]) scheme described in Refs. [38, 41].

The numerical results obtained for the rate constants are shown in the Arrhenius plots displayed in Fig. 2. The values of the parameters α , N , ν , and η are the same used to produce Fig. 1, which means that the inverse of the transition temperature is equal to $\beta^* = 1/RT^* = 0.382271 (\text{kJ/mol})^{-1}$ (with $R = k_B N_A$). Continuous lines denote the fits to the theoretical expressions, Eqs. 7, 8, and 9, from where we got $\Delta E_{-}^{\ddagger} \approx 1.683 \times 10^4 \text{ kJ/mol}$, $\Delta E_{+}^{\ddagger} \approx -1.264 \times 10^4 \text{ kJ/mol}$, and $\Delta E^{\ddagger} \approx 2.947 \times 10^4 \text{ kJ/mol}$, by assuming that the barrier height is given by the microcanonical estimate, *i.e.*, $\beta^* \Delta F^{\ddagger} = 2.813$, and that $\gamma^* \approx 4.2 \times 10^{-8} (\text{kJ/mol})^{-2}$. This fitting

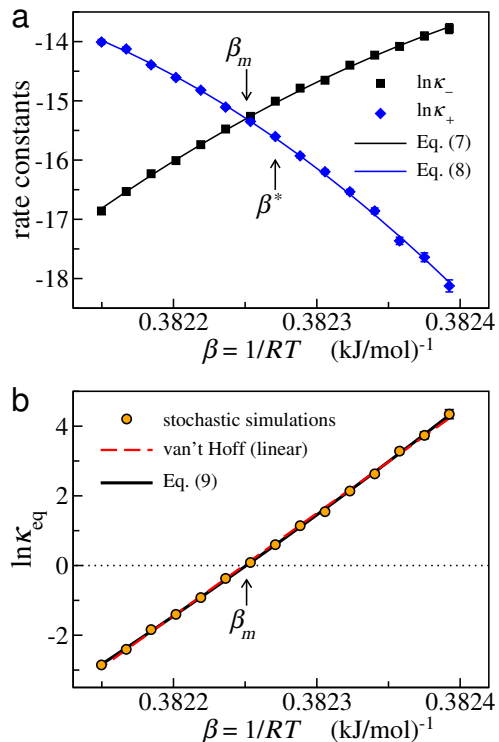


FIG. 2. (a) Arrhenius-plot for the forward κ_{-} and reverse κ_{+} rate constants. (b) Equilibrium rate constant, $\kappa_{\text{eq}} = \kappa_{-}/\kappa_{+}$. Arrows indicate the inverse transition temperature $\beta^* = 1/RT^* = 0.382271 (\text{kJ/mol})^{-1}$, and the inverse midpoint temperature, $\beta_m = 1/RT_m = 0.382251 (\text{kJ/mol})^{-1}$, where $\kappa_{\text{eq}} = 1$. Symbols denote numerical results obtained from the stochastic simulations, while continuous lines correspond to fits to the numerical data. In (b) we also include the fit using the linear van't Hoff's expression (see text).

procedure also yields $\gamma_{-} \approx 3.4 \times 10^{-8} (\text{kJ/mol})^{-2}$ and $\gamma_{+} \approx 11 \times 10^{-8} (\text{kJ/mol})^{-2}$, so that the values of $\bar{\gamma}_{-}$ and $\bar{\gamma}_{+}$ are self-consistent with the pre-factors A_{-} , A_{+} , and A . Importantly, the obtained values for γ_{-} and γ_{+} are also in good agreement with the values one would obtain by considering direct fits of the quadratic approximated expressions to the free-energy profile $\beta^* \Delta F(E)$ at the minima displayed in Fig. 1(c) (in fact, these values were used to plot the dotted curves close to E_{\pm} in that figure).

As noted in Ref. [31], the pre-factors A_{-} and A_{+} may be different if the wells of the free-energy profile are asymmetrical, so that the equilibrium rate κ_{eq} is not necessarily equal to one at the transition temperature T^* . Indeed, the asymmetry observed in the wells of the free-energy profiles $\beta^* \Delta F(E)$ displayed in Fig. 1(c) is consistent with the pre-factor $A = 1.805$ and the positive value found for $\Delta\bar{\gamma} \approx 0.205 \times 10^8 (\text{kJ/mol})^2$, which means that the well close to the energy E_{+} is sharper than the well close to E_{-} (*i.e.*, $\gamma_{-} < \gamma_{+}$). The midpoint transition temperature $T_m = 1/R\beta_m$ can be estimated from Eq. 9 by considering that $\beta_m = \beta^* + \delta$ and imposing that $\kappa_{\text{eq}}(T_m) = 1$, which yields $\delta = (2\Delta E^{\ddagger})^{-1} \ln(\gamma_{-}/\gamma_{+})$. Hence, at $T_m = 314.642 \text{ K}$, one finds that the peaks in

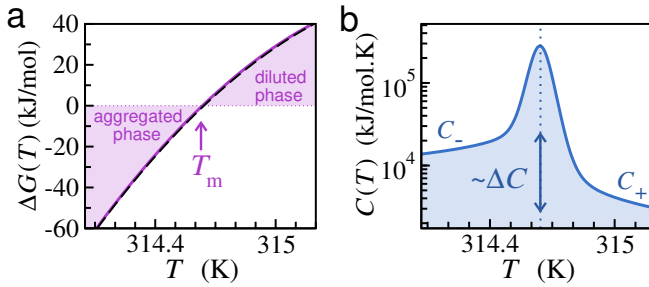


FIG. 3. (a) Effective free-energy $\Delta G(T)$, Eq. 10, obtained with the parameters extracted from Fig. 2, and its numerical fit to Eq. 11 (dashed black line). (b) Heat capacity $C(T)$ close to the transition temperature T_m (dotted line), with $\Delta C < 0$, obtained from the PDF evaluated from the density of states, Eq. 1, with the parameters used in Fig. 1.

$p(E)$ should have the same area under the curve, instead of having maxima with equal heights as at T^* .

It is worth noting that, although the logarithm of the equilibrium rate in Fig. 2(b) seems to display a linear behavior that can be fitted to the usual van't Hoff expression, *i.e.*, $\kappa_{\text{eq}}^\ominus = \exp[\beta\Delta E^\ominus - \Delta S^\ominus/k_B]$, the forward and reverse rates in Fig. 2(a) clearly show non-Arrhenius behaviors. The linear fit to $\ln \kappa_{\text{eq}}$ yields $\Delta E^\ominus = 2.947 \times 10^4$ kJ/mol and $\Delta S^\ominus/k_B = 1.126 \times 10^4$, which are close to the values ΔE^\ddagger and $\Delta S^\ddagger/k_B = \beta^* \Delta E^\ddagger$ obtained from the fit of Eq. 9 to the numerical data. Accordingly, as it is noted in Ref. [31], the values of ΔE^\ddagger and ΔS^\ddagger that are obtained from the kinetic approach are systematically close to the equilibrium values extracted from Fig. 1(c), *i.e.*, $\Delta E^\ddagger \approx 0.9\Delta E^\ddagger$ and $\Delta S^\ddagger \approx 0.9\Delta S^\ddagger$, even though we assume that the energies E_- and E_+ are independent of the temperature. Importantly, the latent heat obtained from the kinetic approach is consistent with the value of the effective interaction energy per bond, *i.e.*, $\Delta E^\ddagger/(NN_A) \sim 5 \times 10^{-21}$ J.

Finally, we include in Fig. 3 the temperature-dependent effective free-energy, $\Delta G(T) = -RT \ln \kappa_{\text{eq}}$, and the heat capacity, $C(T) = (\langle E^2 \rangle - \langle E \rangle^2)/RT^2$, in order to illustrate the relationship between our theory and the thermal analyses that are commonly used to interpret the experimental data [42]. From Eq. 9, we find

$$\Delta G(T) \approx -\Delta E^\ddagger \left(1 - \frac{T}{T_m}\right) - \frac{\Delta \bar{\gamma}}{2RT} \left(1 - \frac{T}{T_m}\right)^2, \quad (10)$$

which can be compared, for instance, with a widely used expression for macromolecular systems given by

$$\Delta G(T) \approx -\Delta E^\ddagger \left(1 - \frac{T}{T_m}\right) - \Delta C \left[(T - T_m) - T \ln \left(\frac{T}{T_m}\right) \right] \quad (11)$$

that is obtained from the assumption that ΔC is an effective temperature-independent change in the heat capacity [43]. Although the latter approximation (Eq. 11) might be poor in some cases, the fit of Eq. 11 to the data displayed in Fig. 3(a) yields $\Delta C \approx -2.3 \times 10^4$ kJ/mol.K,

which can be used to verify that [31] $\Delta C \approx -\Delta \bar{\gamma}/RT_m^2 < 0$ when $T \approx T_m$. Indeed, the behavior of $C(T)$ displayed in Fig. 3(b) for the aggregation transition studied here, *i.e.*, with $C_- > C_+$ and $\Delta C < 0$, is also supported by numerical simulations of more detailed aggregation models [44–47]. Even so, our model-independent kinetic approach can be also applied to study the behavior observed for, *e.g.*, protein folding transitions [48], where one may find that [31] $\Delta C > 0$ and $\Delta \bar{\gamma} < 0$.

In conclusion, we present a shape-free rate theory that allows one to associate equilibrium properties that are determined from an analysis based on the microcanonical entropy $S(N, V, E)$ to the self-assembly kinetics of finite-sized macromolecular and colloidal systems. It is worth mentioning that our approach provides an insightful theoretical interpretation for the temperature-dependent rate constants, *i.e.*, Eqs. 7, 8, and 9, in contrast to the popularly used Arrhenius-like expressions that are based on phenomenological approaches [49, 50]. Hence, we believe that our theory should help experimentalists that work with phase change materials [2] and nucleation phenomena [51, 52] to interpret their results. In particular, one could use the kinetic approach presented here as a reliable method to reconstruct free-energy profiles $\beta^* \Delta F(E)$ and microcanonical entropies $S(E)$ from the experimental kinetic data.

The authors acknowledge the funding by the Brazilian agencies CAPES (code 001), FAPEMIG (Process APQ-02783-18), and CNPq (Grants 306302/2018-7 and 426570/2018-9).

-
- [1] M. F. Hagan, M. Fisher, and G. M. Grason, *Rev. Mod. Phys.* **93**, 025008 (2021).
 - [2] L. Klimeš, P. Charvát, M. M. Joybari, M. Zálezák, F. Haghghat, K. Panchabikesan, M. E. Mankibi, and Y. Yuan, *Appl. Energy* **263**, 114572 (2020).
 - [3] T. P. J. Knowles, M. Vendruscolo, and C. M. Dobson, *Nat. Rev. Mol. Cell. Biol.* **15**, 384 (2014).
 - [4] D. Reguera, R. K. Bowles, Y. Djikaev, and H. Reiss, *J. Chem. Phys.* **118**, 340 (2003).
 - [5] J. Merikanto, E. Zapadinsky, A. Lauri, and H. Vehkamäki, *Phys. Rev. Lett.* **98**, 145702 (2007).
 - [6] Y. Wang, S. J. Bunce, S. E. Radford, A. J. Wilson, S. Auer, and C. K. Hall, *Proc. Natl. Acad. Sci. USA* **116**, 2091 (2019).
 - [7] R. Cabriolu, D. Kashchiev, and S. Auer, *J. Chem. Phys.* **137**, 204903 (2012).
 - [8] R. J. Bingham, L. G. Rizzi, R. Cabriolu, and S. Auer, *J. Chem. Phys.* **139**, 241101 (2013).
 - [9] J. Zierenberg, P. Schierz, and W. Janke, *Nat. Commun.* **8**, 14546 (2017).
 - [10] B. A. Berg and T. Neuhaus, *Phys. Rev. Lett.* **68**, 9 (1992).
 - [11] B. A. Berg, *Comput. Phys. Commun.* **153**, 397 (2003).
 - [12] J. Lee, *Phys. Rev. Lett.* **71**, 211 (1993).
 - [13] F. Wang and D. P. Landau, *Phys. Rev. Lett.* **86**, 2050 (2001).
 - [14] J. Kim, J. E. Straub, and T. Keyes, *Phys. Rev. Lett.* **97**, 050601 (2006).

- [15] J. Kim, T. Keyes, and J. E. Straub, *J. Chem. Phys.* **135**, 061103 (2011).
- [16] L. G. Rizzi and N. A. Alves, *J. Chem. Phys.* **135**, 141101 (2011).
- [17] L. Wang, T. Chen, X. Lin, Y. Liu, and H. Liang, *J. Chem. Phys.* **131**, 244902 (2009).
- [18] M. Möddel, W. Janke, and M. Bachmann, *Phys. Chem. Chem. Phys.* **12**, 11548 (2010).
- [19] S. Schnabel, D. T. Seaton, D. P. Landau, and M. Bachmann, *Phys. Rev. E* **84**, 011127 (2011).
- [20] T. Chen, X. Lin, Y. Liu, and H. Liang, *Phys. Rev. E* **76**, 046110 (2007).
- [21] T. Bereau, M. Bachmann, and M. Deserno, *J. Am. Chem. Soc.* **132**, 13129 (2010).
- [22] R. B. Frigori, L. G. Rizzi, and N. A. Alves, *J. Chem. Phys.* **138**, 015102 (2013).
- [23] N. A. Alves, L. D. Morero, and L. G. Rizzi, *Comput. Phys. Commun.* **191**, 125 (2015).
- [24] T. Chen, X. Lin, Y. Liu, T. Lu, and H. Liang, *Phys. Rev. E* **78**, 056101 (2008).
- [25] M. S. Church, C. E. Ferry, and A. E. van Giessens, *J. Chem. Phys.* **136**, 245102 (2012).
- [26] P. Schierz, J. Zierenberg, and W. Janke, *Phys. Rev. E* **94**, 021301(R) (2016).
- [27] C. Junghans, M. Bachmann, and W. Janke, *Phys. Rev. Lett.* **97**, 218103 (2006).
- [28] C. Junghans, M. Bachmann, and W. Janke, *J. Chem. Phys.* **128**, 085103 (2008).
- [29] R. B. Frigori, *Phys. Rev. E* **90**, 052716 (2014).
- [30] L. F. Trugilho and L. G. Rizzi, *J. Phys.: Conf. Ser.* **1483**, 012011 (2020).
- [31] L. G. Rizzi, *J. Stat. Mech.*, 083204 (2020).
- [32] K. Qi and M. Bachmann, *Phys. Rev. Lett.* **120**, 180601 (2018).
- [33] A. Campa, L. Casetti, I. Latella, A. Pérez-Madrid, and S. Ruffo, *J. Stat. Mech.*, 073205 (2016).
- [34] L. F. Trugilho and L. G. Rizzi, in preparation (2021).
- [35] I. Latella, A. Pérez-Madrid, A. Campa, L. Casetti, and S. Ruffo, *Phys. Rev. Lett.* **114**, 230601 (2015).
- [36] W. Thirring, *Z. Phys.* **235**, 339 (1970).
- [37] D. B. Chesnut, *Am. J. Phys.* **52**, 299 (1984).
- [38] W. Nadler and U. H. E. Hansmann, *Phys. Rev. E* **75**, 026109 (2007).
- [39] A. M. Berezhkovskii and A. Szabo, *J. Phys. Chem.* **150**, 054106 (2019).
- [40] The partition function should be evaluated with the large number summation technique presented in Ref. [11]. In principle, instead of $\Omega(E_j)$ one should use the number of microstates $\omega(E_j)$ with energies in the range $[E_j, E_{j+1}[$, but we find no differences between the results obtained from these two definitions for the aggregation model discussed here.
- [41] S. Trebst, D. A. Huse, and M. Troyer, *Phys. Rev. E* **70**, 046701 (2004).
- [42] G. W. H. Höhne, W. F. Hemminger, and H.-J. Flammersheim, *Differential Scanning Calorimetry* (Springer, 2003).
- [43] R. L. Baldwin, *Proc. Natl. Acad. Sci. USA* **83**, 8069 (1986).
- [44] A. Irbäck, S. Jónsson, N. Linnemann, B. Linse, and S. Wallin, *Phys. Rev. Lett.* **110**, 058101 (2013).
- [45] A. Irbäck and J. Wessén, *J. Chem. Phys.* **143**, 105104 (2015).
- [46] A. Nußbaumer, J. Zierenberg, E. Bittner, and W. Janke, *J. Phys.: Conf. Ser.* **759**, 012009 (2016).
- [47] W. Janke, P. Schierz, and J. Zierenberg, *J. Phys.: Conf. Ser.* **921**, 012018 (2017).
- [48] A. Cooper, *J. Phys. Chem. Lett.* **1**, 3298 (2010).
- [49] K. J. Laidler, *J. Chem. Educ.* **61**, 494 (1984).
- [50] J. H. van't Hoff, *Lectures on Theoretical and Physical Chemistry: Part I, Chemical Dynamics* (London: Edward Arnold, 1899).
- [51] R. P. Sear, *J. Phys.: Condens. Matter* **19**, 033101 (2007).
- [52] P. G. Vekilov, *Prog. Cryst. Growth Charact. Mater.* **62**, 136 (2016).